International Journal of Coal Geology 121 (2014) 1–13

Contents lists available at ScienceDirect

International Journal of Coal Geology

journal homepage: www.elsevier.com/locate/ijcoalgeo

Simulation of hydraulic fracturing using particle flow method and application in a coal mine

Tao Wang [a,*], Weibo Zhou [a], Jinhua Chen [b], Xiong Xiao [a], Yang Li [a], Xianyu Zhao [a]

[a] State Key Laboratory of Water Resources and Hydropower Engineering Science, Wuhan University, China
[b] National Key Laboratory of Gas Disaster Detecting, Preventing and Emergency Controlling, Chongqing, China

ARTICLE INFO

Article history:
Received 25 July 2013
Received in revised form 26 October 2013
Accepted 26 October 2013
Available online 6 November 2013

Keywords:
Hydraulic fracturing
Particle flow method
Distinct element method
Coal seam

ABSTRACT

The purpose of hydraulic fracturing is to improve the gas permeability of a coal seam by the high-pressure injection of fracturing fluid into cracks. This paper simulates the hydraulic fracturing of a coal seam, investigates relevant parameters and analyzes the connection between macroscopic mechanical parameters and mesoscopic mechanical parameters based on two-dimensional particle flow code (PFC^{2D}). Furthermore, the influence of macroscopic mechanical properties on the initiation and size of cracks is studied based on various combinations of particle flow calculations. Empirical formulae for the breakdown pressure and fracture radius are derived. Moreover, the effect of the injection parameters on crack propagation is computed and analyzed, after which the relevant empirical formula is proposed. Finally, numerical simulation of the working face N3704 at Yuyang Coal Mine (YCM) is conducted, and the comparison of results from simulation, empirical formulae and field observation is investigated. The research findings of this paper may provide a reference for selecting injection parameters and forecasting the effect in practical hydraulic fracturing applications.

1. Introduction

Hydraulic fracturing (HF) can be defined as the process by which a fracture is initiated and propagates because of hydraulic loading applied by fluid inside the fracture. Today, HF is used extensively in the petroleum industry to stimulate oil and gas wells to increase their productivity (Adachi et al., 2007). Field-scale hydraulic fracturing experiments and research in vertical boreholes have been performed (Cai et al., 2006; Jeffrey et al., 1994; Rahim et al., 1995). Jeffrey and Mills (2000) have described the first successful use of hydraulic fracturing to induce a goaf event and to control the timing of caving events. Cipolla and Wright (2000) have detailed the state of the art in applying both conventional and advanced technologies to better understand hydraulic fracturing and improve treatment designs.

The fundamental principle of HF in a coal seam is the high-pressure injection of fracturing fluid into cracks, including preexisting cracks and artificially induced cracks. During the fracturing period, breakdown pressure is achieved, and the cracks are broadened, extended and combined. Wright and Conant (1995) have stated that the hydraulic fracture orientation is critical to both primary and secondary oil recoveries. Abass et al. (1992) have designed experiments to investigate nonplanar fracture geometries. As a result of HF, the number of interconnected cracks and the apertures are increased significantly. Furthermore, many artificially induced cracks appear, and the gas permeability is increased. Meanwhile, high-pressure fluid is able to extrude gas in the coal seam, which forces free and absorbed gas in the vicinity of the borehole to increase the total volume of gas collected. However, during the production of HF in a coal seam, some treatments can produce predetermined effects, while others cannot. The main reason for this lack of predictability is the inadequate research regarding the crack-propagation mechanism of HF, which results in the improper selection of parameters and technical measures. Therefore, sufficient fracturing effects cannot be guaranteed.

The criterion for fracture propagation is usually according to the conventional energy-release-rate approach of the linear elastic fracture mechanics (LEFM) theory. There are increasing evidences from the direct monitoring of field treatments suggesting that fracture can grow in a complicated manner, taking advantage of local heterogeneities, layering, and natural fracture networks in the reservoir. These effects complicate the design of treatments and make numerical modeling far more challenging (Adachi et al., 2007). Because of the complexity of the elastic-plastic fracture properties of a coal seam, the solutions to most problems will depend on numerical simulation analysis, although analytical solutions can rarely be obtained except under certain conditions. On the basis of the mine back work performed in the 1970s and 1980s at the Nevada test site, it is clear that hydraulic fractures are much more complex than envisioned by conventional modes of the process (Fisher and Warpinski, 2012; Warpinski, 1985). To better understand the mechanics of HF, a large amount of research has been carried out in the past few decades, and various numerical analysis techniques have been applied.

The Finite Element Method (FEM) and the Boundary Element Method (BEM) have been used to simulate HF in complex structures

* Corresponding author. Tel.: +86 27 68773941, +86 13871511155 (mobile).
E-mail address: htwang@whu.edu.cn (T. Wang).

0166-5162/$ – see front matter
http://dx.doi.org/10.1016/j.coal.2013.10.012

(Papanastasiou, 1997; Vychytil and Horii, 1998). The mathematical formulae for an overall fracture propagation model require the coupling of a set of complex equations, thus necessitating the development of sophisticated numerical tools based on FEM or BEM. Because fracture propagation is mainly controlled by the stress singularity at the fracture tip, it is sufficient to consider problems at the fracture boundary rather than throughout the entire region, as considered in FEM. Hence, the BEM is usually considered to be more suitable. On the other hand, the fluid-flow equation can be more conveniently solved using the FEM. Therefore, the overall calculation time to solve a fluid-pressure-driven fracture-propagation problem can be reduced significantly by combining these two numerical methods (Hossain and Rahman, 2008).

The estimation or determination of fracture geometry has been one of the most difficult technical challenges in HF treatment. Papanastasiou (1997) has presented a fully coupled elastic-plastic hydraulic fracturing model based on FEM analysis. Hoffman and Chang (2009) have demonstrated how to capture more complexity and model these systems using a finite-difference simulator. The mechanical response of rock masses to high-pressure hydraulic injections applied during a hot dry rock stimulation has been studied, and the variation of the mechanical response under different geological conditions has been demonstrated using FEM analysis (Vychytil and Horii, 1998). The propagation of HF in coal seams under high-pressure water has been simulated using RFPA-Flow based on the maximum tensile strain criterion (Du et al., 2008). A three-dimensional nonlinear fluid-mechanics coupling FEM has been established based on the FEM software ABAQUS. The staged fracturing process of a horizontal well in Daqing Oilfield has been simulated using this model (Zhang et al., 2010). A FEM numerical model has been used to simulate the fully coupled gas flow and stress changes of a hydraulically fractured and refractured tight-gas reservoir (Aghighi and Rahman, 2010). Wang et al. (2010) have proposed a coupled algorithm of FEM and a meshless method for the simulation of the dynamic propagation of cracking under either external forces or hydraulic pressure.

Some researchers have also introduced the discrete element method (DEM) technique for the simulation of HF. Al-Busaidi et al. (2005) have simulated hydraulic fracturing in granite using the DEM, and the results were compared to the experimental acoustic emission data from the experiment. Shimizu (2010) and Shimizu et al. (2011) have performed a series of simulations of HF in competent rock using a flow-coupled DEM code to investigate the influence of the fluid viscosity and the particle-size distribution. Han et al. (2012) have simulated the interaction between the natural fractures and hydraulic fracturing through PFC. McLennan et al. (2010) have described an approach to representing and assessing complex fracture growth and associated production prediction through the generated fracture using the DEM.

Particle flow distinct element methods have become an effective tool for modeling crack propagation though they are not perfect enough (Potyondy and Cundall, 2004). However, there is little or no information available in the literature concerned with the systematic study of the HF mechanism in coal based on this method. In this paper, the two dimensional particle flow code (PFC^{2D}) (Itasca, 2010) was used to simulate the HF process of a coal seam. The connection between the mechanical parameters of different scales, the correlations among the injection parameters and the performance of cracks induced by HF were all studied. The objectives of this work are to investigate the trends governing crack propagation in a coal seam, to propose schemes that could achieve the desired fracturing effects, and to aid in optimally guiding engineering practices.

2. Simulation mechanism using PFC

Particle-flow code (PFC) models the movement and interaction of circular particles using the DEM, as described by Cundall and Strack (1979). PFC has three advantages. First, it is potentially more efficient, as contact detection between circular objects is much simpler than contact detection between angular objects; second, there is essentially no limit to the extent of displacement that can be modeled; and third, it is possible for the blocks to break (because they are composed of bonded particles) (Itasca, 2010). The constitutive behavior of a material is simulated in PFC by associating a contact model with each contact (see Fig. 1). A parallel bond can be envisioned as a set of elastic springs uniformly distributed over a rectangular cross section lying on the contact plane and centered at the contact point. These springs act in parallel with the point-contact springs (which come into play when two particles overlap).

The rock material is modeled as a collection of rounded particles that can interact via normal and shear springs. Thus, HF can be modeled by assuming that a rock is made up of individual particles of specific stiffness bonded with bonds of specific strength. Under the applied load, the bonds between the particles can break, and a small crack can form. The crack pattern is developed automatically with no need for remeshing. The calculation cycle in PFC is a time-stepping algorithm that requires the repeated application of the law of motion for each particle and a force-displacement law for each contact (Al-Busaidi et al., 2005).

Particles in PFC are free to move in the normal and shear directions and can also rotate relative to other particles. This rotation may induce a moment between particles, but the contact bond model cannot resist this moment. With the parallel bond model however, bonding is activated over a finite area, and this bonding can therefore resist a moment, as illustrated in Fig. 1. In the contact bond model, the contact stiffness remains even after bond breakage as long as the particles remain in contact. This implies that in a contact bond model, if particle contact is maintained, bond breakage may not significantly affect the macro-stiffness, which is unlikely in rocks. In the parallel bond model, however, stiffness is contributed by both contact stiffness and bond stiffness. Thus, bond breakage in the parallel model immediately results in a stiffness reduction, which not only affects the stiffness of adjacent assemblies but also affects the macro-stiffness of the particle assembly. From this standpoint, the parallel bond model is a more realistic bond model for rock-like materials, in which the bonds may break because of either tension or shearing, with an associated decline in stiffness. For these reasons, the parallel model was used in the study presented in this paper.

2.1. Fluid-mechanical coupling theory of PFC

When the coupling of the stress field and the seepage field in a jointed rock mass is numerically simulated, both fields should be considered. It is difficult to reflect the formation and propagation of cracks in such a coupling process. At present, a numerical simulation software based on FEM and BEM is not fully able to consider both contributions, and the use of these methods in modeling the coupling of the stress field and the seepage field for a fissured rock mass is immature. However, PFC is able to solve the problems mentioned effectively because of its distinctive characteristics.

Early DEMs were not able to consider the fluid flow between particles or blocks (Cundall, 1971; Cundall and Strack, 1979). Lemos and Lorig (1990) have provided a description of the steady-state and transient fluid-flow modeling in blocks as well as confined flow and flow with a free surface. Tsuji et al. (1992) have applied the Ergun equation to obtain the fluid force acting on particles in a moving or stationary bed. The method of particle/fluid interaction in PFC was developed by Prof. Tsuji (Itasca, 2010; Tsuji et al., 1993). A particle-fluid coupling scheme with a mixed Lagrangian–Euler approach has been used to describe particle–fluid interactions (Shimizu, 2004). Fluid flow in the pore space has been explicitly modeled at the mesoscopic level using the lattice Boltzmann method; the geometrical representation and the mechanical behavior of the solid skeleton have been modeled at the microscopic level using the PFC method (Han and Cundall, 2011, 2013).

The seepage effect can be modeled by adopting a fluid “domain” and fluid “pipe” (see Fig. 2). A “domain” is defined as a closed chain of

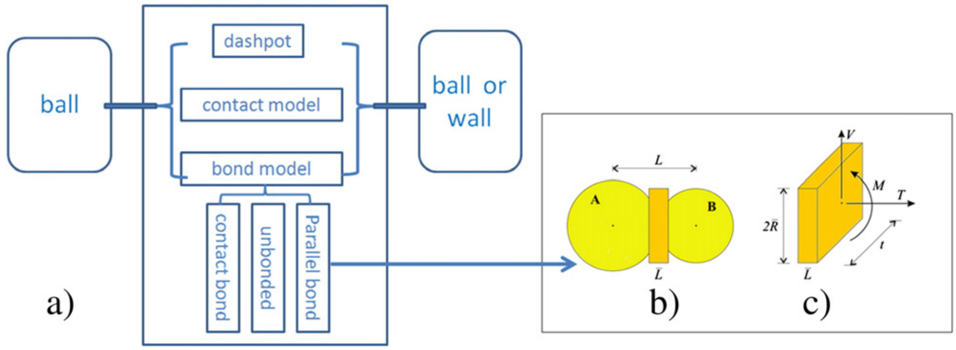

Fig. 1. Contact and a parallel bond in PFC^{2D} (components of a contact (a), parallel bond model (b) and the forces carried in the 2D bond material (c)). Modified from (Itasca, 2010).

particles, in which each link in the chain is a bonded contact. Each domain holds a pointer, via which all domains become connected (Itasca, 2010). Meanwhile, a "pipe" is not only a fluid channel in a solid but also a channel connecting a "domain," which is considered to be tangential to each ball at the location of the bond contact. The aperture of a "pipe" is in direct proportion to the normal displacement of the contact. It changes when the contact breaks or the particle moves, under the condition that the particles are mutually connected initially. The volume of a "domain" is related to the number and apertures of the surrounding pipes. In addition, the water pressure in the "domain" continually changes as the coupling calculation proceeds, and it is applied to each particle as a body force.

As shown in Fig. 2, each channel is assumed to be a set of parallel plates with some aperture, and the fluid flow in the channel is modeled using the Poiseuille equation. In the figure, f_c is the total force acting on the plate. Therefore, the volumetric laminar-flow rate q is given by the following equation:

$$q = \frac{a^3}{12\mu}\frac{\Delta p}{L} \tag{1}$$

where a is the aperture, L is the length of the channel, Δp is the pressure difference between the two neighboring domains, and μ is the viscosity of the fluid. The out-of-plane thickness is assumed to be of unit length.

Each domain gathers the fluid pressure acting on the surfaces of the surrounding particles, and the fluid pressure is updated during the

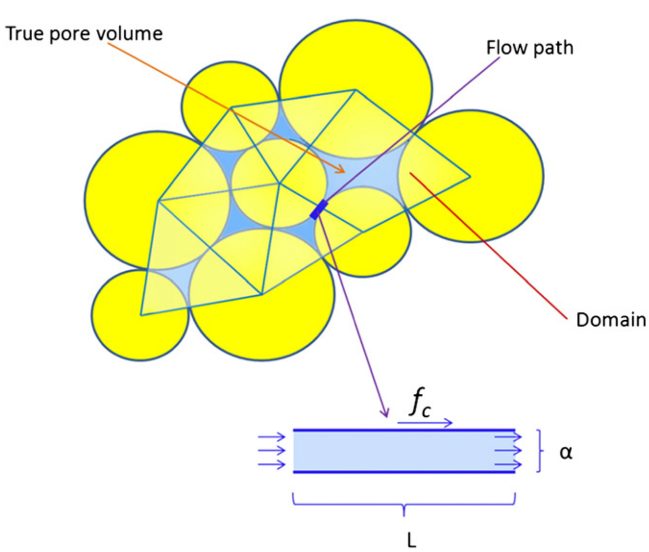

Fig. 2. Domains and flow paths in a bonded assembly of particles.

fluid-flow calculation. The change in the fluid pressure Δp is given by the following continuity equation (Shimizu, 2010; Shimizu et al., 2011):

$$\Delta p = \frac{K_f}{V_d}(\Sigma q \Delta t - \Delta V_d) \tag{2}$$

where $\sum q$ is the total flow rate for one time step. Δt is the duration of one time step. K_f is the fluid bulk modulus, and V_d is the volume of the domain. ΔV_d is the change in the volume of the domain.

At each time step, mechanical computations determine the geometry of the system, thus producing the new aperture values for all particles and volume values for all domains. The flow rates through the particles can then be calculated. Then, the domain pressures are updated. Given the new domain pressures, the force exerted by the fluid on the edges of the surrounding particles can be obtained (Lemos, 1987; Lemos and Lorig, 1990). Consider a pressure perturbation in a single domain. The flow into the domain caused by the pressure perturbation Δp_p can then be calculated from Eq. (1) as follows:

$$q = \frac{Na^3 \Delta p_p}{24\mu R} \tag{3}$$

where R is the mean radius of the particles surrounding the domain, N is the number of pipes connected to the domain, and Δp_p is a pressure response caused by the flow. This last quantity can be written as follows:

$$\Delta p_p = \frac{K_f q \Delta t}{V_d}. \tag{4}$$

Using PFC to simulate coupled seepage and stress fields, we can actually consider the model as a binary-medium model. In the model, it is suggested that pores and cracks act as containers for water storage and channels for water conduction, respectively. Because of the water-conduction effect, there exist two water heads in this binary-medium model, namely, a water head in a porous medium and one in a fissured medium. The two media are connected via the water exchange between them.

2.2. Crack-growth theory in PFC

Potyondy and Cundall (2004) have classified computational models of rock into two categories depending on whether the damage is represented indirectly, by its effect on constitutive relations, or directly, by the formation and tracking of many microcracks. Most indirect approaches conceptualize the material as a continuum and use average measures of material degradation in constitutive relations to represent irreversible microstructural damage (Krajcinovic, 2000), while most direct approaches conceptualize the material as a collection of structural units (springs, beams, etc.) or separate particles bonded together at their contact points and use the breakage of individual structural units or bonds to represent damage (Schlangen and Garboczi, 1997).

Shimizu (2010) has noted that in traditional simulation algorithms, such as FEM and BEM, that rely on a grid or a mesh, adaptive techniques and complex remeshing procedures are needed to treat nonlinear material behaviors such as microcrack generation, large deformation and the propagation of arbitrarily complex crack paths. The behavior of the parallel-bond springs is similar to that of a beam. Relative motion at the parallel-bonded contact causes axial- and shear-directed forces (T and V, respectively) and a moment (M) to develop. As shown in Fig. 1, the maximum tensile and shear stresses acting on the bond edge are calculated to be

$$\begin{aligned} \sigma_{\max} &= \frac{T}{A} + \frac{|M|}{I}\overline{R} \\ \tau_{\max} &= \frac{|V|}{A} \end{aligned} \tag{5}$$

where A is the area of the bond cross section, I is the moment of inertia of the bond cross section, and $\overline{R}$ is the bond radius (see Fig. 1). If the maximum tensile stress exceeds the normal strength ($\sigma_{\max} \geq \overline{\sigma}_c$) or the maximum shear stress exceeds the shear strength ($\tau_{\max} \geq \overline{\tau}_c$), then the parallel bond breaks (Itasca, 2010).

In PFC bond rupture, a crack forms when the shear or tensile force reaches the specified bond strength. When the bond rupture is tensile, the bond tensile strength immediately drops to zero. In shear bond rupture, the strength reduces to a residual value that is a function of the normal stress and the coefficient of friction acting at the contact (Cho et al., 2007).

3. Determination of mesoscopic parameters

The proper selection of meso-mechanical parameters is the key to simulation using PFC. Based on the correlation between the macro-mechanical parameters of a particle assembly and the meso-mechanical parameters of a particle, meso-mechanical parameters can be determined by conducting numerical simulations of physical mechanics in PFC^{2D} and the regression analysis of the corresponding simulation results. Among conventional rock-mechanics tests, the macro-elastic modulus, the Poisson's ratio and the uniaxial compressive strength (UCS) can be obtained via a uniaxial compression test. Meanwhile, via a Brazilian disc test, the tensile strength can be determined. In this work, both numerical tests (see Fig. 3) were conducted to study the connections among particle parameters on different scales. Based on the parallel-bond model, this paper provides empirical formulae relating the macro-mechanical parameters of a material, such as the macro-elastic modulus (E), Poisson's ratio (v), the UCS (σ_c), and the tensile strength (σ_t), and the meso-mechanical parameters of the material's constituent particles, such as Young's modulus (E_c) of a particle–particle contact or parallel-bond contact, the normal-to-shear stiffness ratio (k_n/k_s) of the particle–particle or parallel-bond contact, and the normal and shear strengths of a parallel bond ($\overline{\sigma}, \overline{\tau}$).

3.1. Numerical calibration models

There are two types of mesoscopic parameters to be determined in PFC, i.e., the deformability and strength parameters. These mesoscopic parameters can be calibrated using the uniaxial compression test and the Brazilian disc test. As shown in Fig. 3 and Table 1, a model of 5 cm in width and 10 cm in height was used to simulate the uniaxial compression test, and a model of 5 cm in diameter was used to simulate the Brazilian disc test. The coal model was expressed as an assembly of particles bonded with each other. The particle radius was chosen to have a uniform distribution between the maximum and minimum radii. The minimum radius is 0.5 mm, the ratio of the largest radius to the smallest radius is 1.66, and the porosity is 0.15.

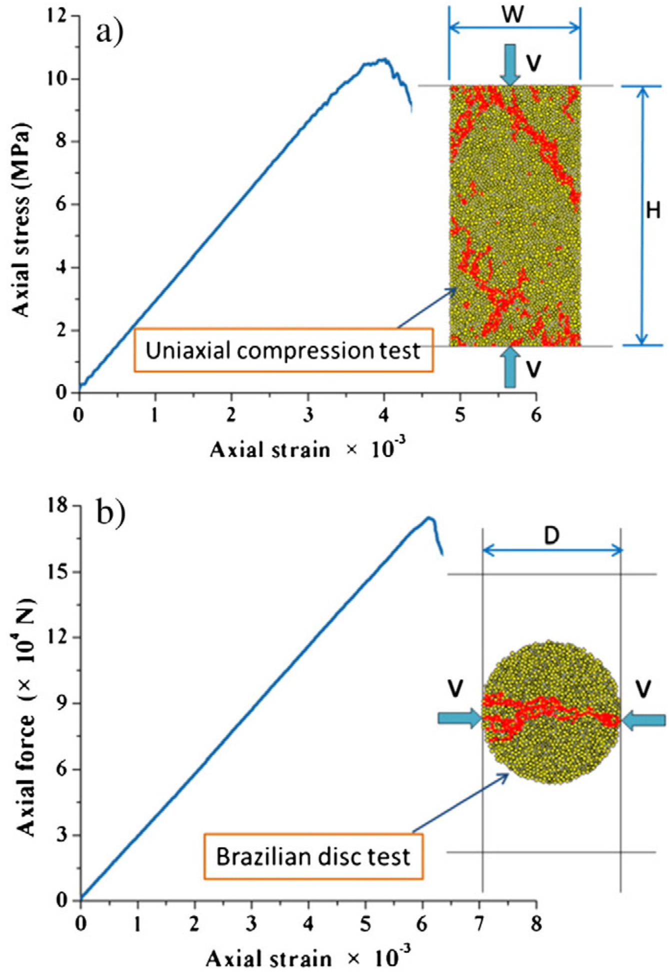

Fig. 3. Simulated PFC^{2D} failure during a uniaxial compression test (a) and a Brazilian disc test (b) (red lines indicate cracks).

The number of particles was 3311 in the uniaxial compression test model and 1306 in the Brazilian disc test model. The density of particles is 1635 kg/m^3, and the particle friction coefficient is 0.71. The walls above and below the model were moved slowly at a velocity of 0.05 m/s to simulate the uniaxial compression test. The axial stresses of the walls and the axial and lateral strains were monitored. In the Brazilian disc model, the upper and lower walls were fixed; the left and right walls were moved at a velocity of 0.025 m/s. The load effect on the walls was recorded.

3.2. Identification of deformability parameters

The deformability parameters include the meso-Young's modulus and the ratio of normal stiffness to shear stiffness. These meso-mechanical

Table 1
Basic parameters for calculations.

Parameter	Uniaxial compression test	Brazilian disk test
Sample size (m)	Width × Height = 0.05 × 0.1	Diameter × Thickness = 0.05 × 1
Minimum of particle radius (mm)	0.5	0.5
Ratio of largest radius to smallest	1.66	1.66
Porosity	0.15	0.15
Number of particles	3311	1306
Particle density (kg/m^3)	1635	1635

parameters were calibrated to match the material's macro-mechanical parameters – the macro-elastic modulus and Poisson's ratio – which were determined from the numerical uniaxial compression tests.

As seen in Figs. 4 and 5, the material's macro-elastic modulus is related to the meso-Young's modulus at each particle–particle contact and parallel-bond contact (assuming that the two modulus values are the same) and to the normal-to-shear stiffness ratio of the particle–particle and parallel-bond contacts (assuming that the two ratios are the same). When the ratio is kept constant, the macro-elastic modulus increases linearly with the meso-Young's modulus. When the meso-Young's modulus is fixed, as the ratio increases, the macro-elastic modulus decreases. Based on these findings, when regression analysis of the simulation results was conducted, a functional relationship was obtained as shown in Eq. (6), and its correlation coefficient was found to be 0.993. The results from the regression analysis and the numerical simulation are shown in Fig. 6. It can be concluded that the fit quality is high.

After analysis of a large number of uniaxial compression tests, it was found that Poisson's ratio primarily depends on the ratio. Fig. 7 shows Poisson's ratio as a function of the normal-to-shear stiffness ratio. As the ratio increases, Poisson's ratio also increases. The regression fitting formula for Poisson's ratio is shown in Eq. (7), and its correlation coefficient was found to be 0.997. A comparison between the fitting curve and the numerical test results is shown in Fig. 7.

$$^{E}\!/_{E_c} = a + b\ln\left(^{k_n}\!/_{k_s}\right) \tag{6}$$

$$v = c\ln\left(^{k_n}\!/_{k_s}\right) + d \tag{7}$$

where $a = 1.652$, $b = -0.395$, $c = 0.209$, and $d = 0.111$.

3.3. Identification of strength parameters

The mesoscopic strength parameters include the normal strength ($\overline{\sigma}$) and shear strength ($\overline{\tau}$) of a parallel bond. The destruction of parallel bonds depends on these mesoscopic strengths, which is to say that these quantities determine whether meso-cracks appear during numerical simulations. The initiation, propagation and linkage of a large number of cracks will result in the macro failure of the sample. The influence of the mesoscopic strengths on the UCS and tensile strength was investigated using the uniaxial compression test and the Brazilian disc test.

The results are shown in Fig. 8. The UCS is related to the ratio $\overline{\tau}/\overline{\sigma}$. When $0<\overline{\tau}/\overline{\sigma}\leq 1$, $\sigma_c/\overline{\sigma}$ initially increases linearly as $\overline{\tau}/\overline{\sigma}$ increases, but the rate of increase of $\sigma_c/\overline{\sigma}$ becomes progressively smaller as $\overline{\tau}/\overline{\sigma}$ approaches 1. It was found that the relationship between $\sigma_c/\overline{\sigma}$ and $\overline{\tau}/\overline{\sigma}$ takes the form of a quadratic parabola. When $\overline{\tau}/\overline{\sigma}>1$, the UCS is mainly determined by the parallel-bond normal strength and increases linearly with it. Even if the value of shear strength is great, $\sigma_c/\overline{\sigma}$ remains constant. The tensile strength exhibits a similar trend as the UCS (Fig. 9). The regression formulae are shown in Eqs. (8) and (9). The correlation coefficients were found to be 0.998 and 0.996, respectively.

$$\frac{\sigma_c}{\overline{\sigma}} = \begin{cases} a\left(\frac{\overline{\tau}}{\overline{\sigma}}\right)^2 + b\frac{\overline{\tau}}{\overline{\sigma}} \quad , & 0<\frac{\overline{\tau}}{\overline{\sigma}}\leq 1 \\ c \quad , & \frac{\overline{\tau}}{\overline{\sigma}}\geq 1 \end{cases} \tag{8}$$

$$\frac{\sigma_t}{\overline{\sigma}} = \begin{cases} d\left(\frac{\overline{\tau}}{\overline{\sigma}}\right)^2 + e\frac{\overline{\tau}}{\overline{\sigma}} \quad , & 0<\frac{\overline{\tau}}{\overline{\sigma}}\leq 1 \\ f \quad , & \frac{\overline{\tau}}{\overline{\sigma}}\geq 1 \end{cases} \tag{9}$$

where $a = -0.965$, $b = 2.292$, $c = 1.327$, $d = -0.174$, $e = 0.463$, and $f = 0.289$.

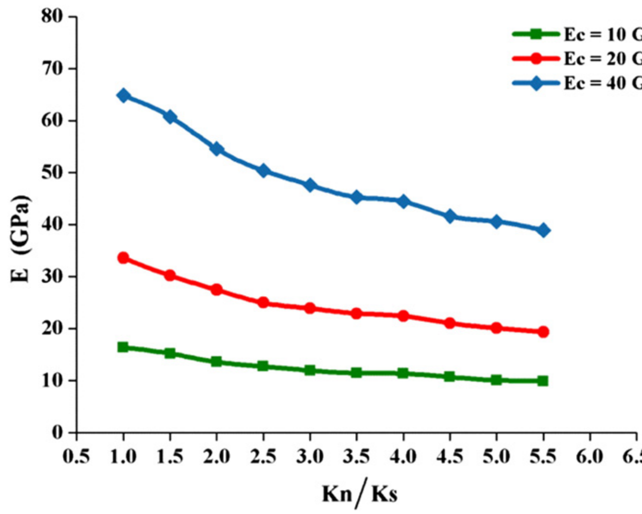

Fig. 5. Macro-elastic modulus vs. stiffness ratio for various values of the meso-Young's modulus.

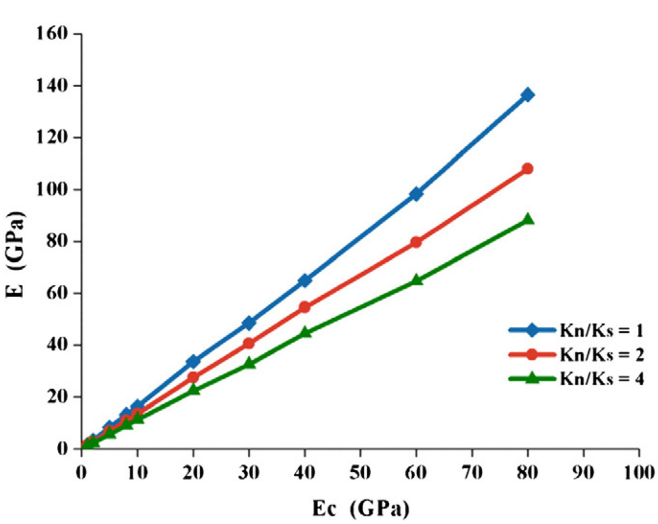

Fig. 4. Macro-elastic modulus vs. meso-Young's modulus for various stiffness ratios.

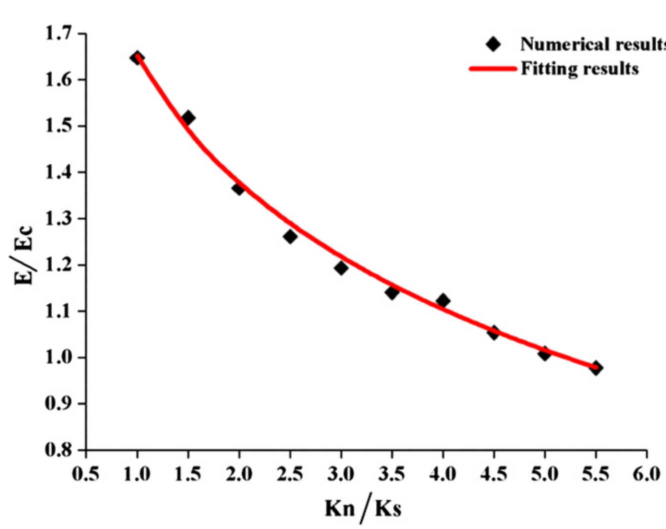

Fig. 6. Simulated relationship between modulus ratio and stiffness ratio.

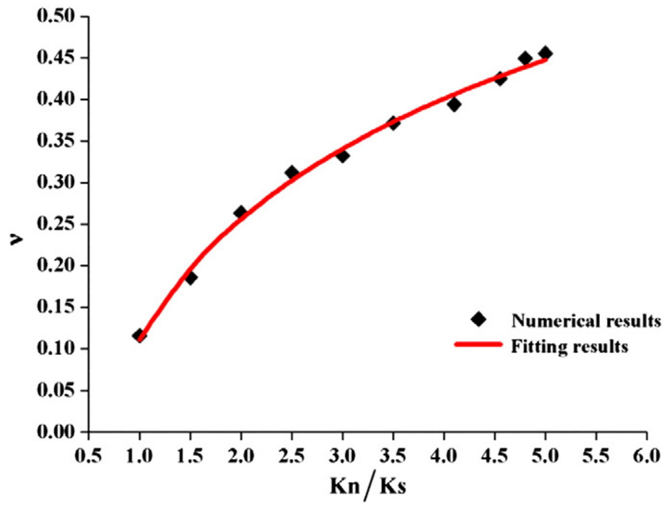

Fig. 7. Simulated relationship between Poisson's ratio and stiffness ratio.

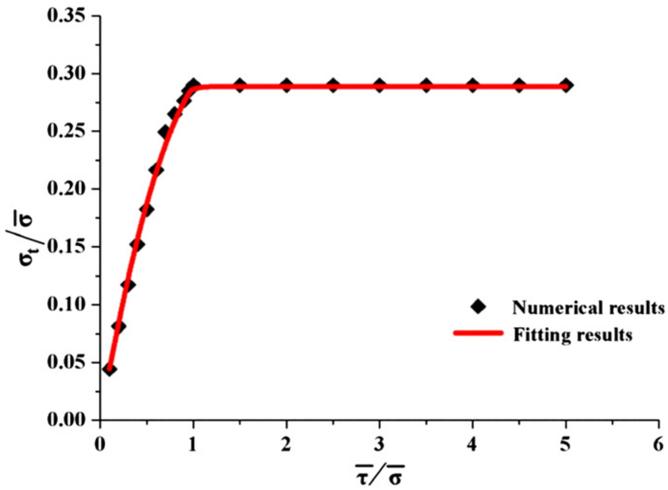

Fig. 9. Fitting results of the tensile strength from numerical calculations.

3.4. Parameter calibration procedure

The material properties determined via laboratory tests are macro-mechanical in nature, as they reflect continuum behavior. An inverse modeling procedure was used to extract suitable meso-mechanical parameters for the numerical models from the macro-mechanical parameters determined in the laboratory tests. This is a trial-and-error approach, as no theory exists that relates these two sets of material properties (Kulatilake et al., 2001; Wang, 2008; Wang and Tonon, 2009). An optimization approach has been devised for calibrating contact-bonded particle models in uniaxial compression simulations (Yoon, 2007). Artificial neural networks have been used to predict the micro-properties of particle flow code in three dimensional particle flow code (PFC^{3D}) models (Tawadrous et al., 2009). In this work, numerical experiments were carried out by applying various comparison schemes. The connections among the macro-mechanical parameters and the meso-mechanical parameters were established based on regression analysis. The analytical formulae were used to select meso-mechanical parameters for the following study. According to the established functions, preliminary values of the meso-mechanical parameters were determined. These values were fine-tuned repeatedly and taken as references to perform corresponding numerical tests. The final meso-mechanical parameters were determined by repeating this process until the differences between the obtained macro-mechanical parameters and the required values lay within a certain error range. It can be seen in Table 2 that the values of the macro-mechanical parameters measured from the physical tests and the values from the PFC^{2D} numerical tests are close, as are the values of the meso-mechanical parameters calibrated using the PFC^{2D} numerical tests and calculated using empirical formulae (Eqs. (6) to (9)). The correctness and applicability of the empirical formulae have thus been verified. Potyondy and Cundall (2004) have pointed that the strength of the PFC model only matches the UCS, and the Brazilian strength is too high when they simulate the behaviors of the Lac du Bonnet granite. In our work, the tensile strength from the PFC model matches that from physical test well. The possible reason is that the coal belongs to soft rock.

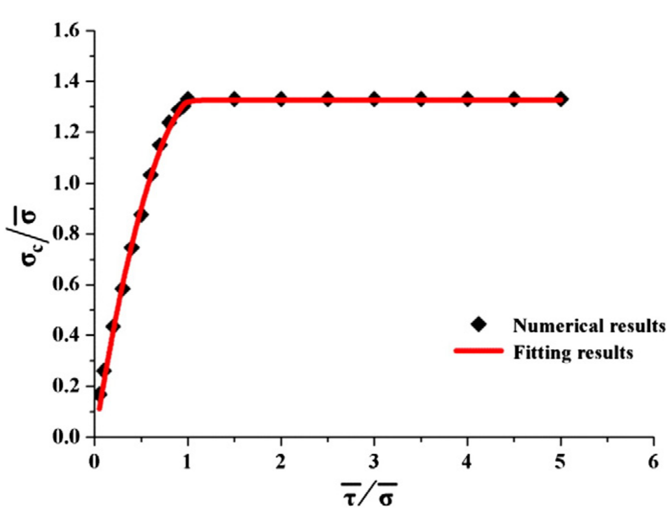

Fig. 8. Fitting results of the UCS from numerical calculations.

4. Effect of macro-mechanical parameters on HF

HF of a coal seam is a gradual injection process that involves wetting, crushing of the coal and the extrusion of the coal gas. It has two main aspects, the crack initiation and the crack propagation within the coal seam, which are not only related to essential internal factors, such as the mechanical properties of the coal seam and initial stress conditions, but are also associated with external technological factors such as the injection flow rate and injection time (Abass et al., 1990; Geertsma and de Klerk, 1969; Li et al., 2010). Assuming certain injection conditions, the initial stress parameters and the tensile strength of the coal

Table 2
Comparisons between the calculated and calibrated meso-mechanical parameters and between the measured and simulated macro-mechanical parameters.

Meso-mechanical parameters	Values calculated using empirical formulae	Calibrated values from PFC^{2D}	Error
Ball-contact Young's modulus (GPa)	2.36	2.4	2%
Parallel-bond Young's modulus (GPa)	2.36	2.4	2%
Parallel-bond shear strength (MPa)	6.92	7.0	1%
Parallel-bond normal strength (MPa)	6.92	7.0	1%
Ball-contact normal-to-shear stiffness ratio	2.7	2.5	8%
Parallel-bond normal-to-shear stiffness ratio	2.7	2.5	8%
Macro-mechanical parameters	**Measured values from physical tests**	**Values from PFC^{2D} assembly**	**Error**
Elastic modulus (GPa)	2.97	3.06	3%
Poisson's ratio	0.32	0.31	3%
UCS (MPa)	10.30	10.46	2%
Tensile strength (MPa)	2.00	1.98	1%

seam were selected as research variables to analyze their influence on the breakdown pressure. The macro-elastic modulus, Poisson's ratio, the UCS and the tensile strength were varied to investigate their effect on the fracture radius.

The numerical calculation model, which is a horizontal plane, is presented in Fig. 10. The model is 50 m in length and width. The particle radius was chosen to have a uniform distribution between the maximum and minimum radii. The minimum radius is 0.42 m, the ratio of the largest to the smallest radius is 1.66, and the porosity is 0.15. The number of particles in the model is 2346. A numerical servo-control was used to adjust the wall velocities to simulate the initial stress. The injection hole for the fracturing was placed in the middle of the model (blue point in Fig. 10). The initial pore pressure was set at the beginning of the calculation, and then fluid was injected with a constant flow. The injection-pressure history curve was constructed by recording the pressure near the injection hole. The fluid-mechanical coupling calculation was performed following the discussion presented in Section 2.1, and the crack calculation was performed in accordance with Section 2.2.

4.1. Major factors influencing the breakdown pressure

According to previous work, the breakdown pressure of the coal seam is primarily associated with the initial stress conditions and the tensile strength of the coal seam (Hubbert and Willis, 1957). The stress ratio (σ_1/σ_2), minimum horizontal principal stress (σ_2), tensile strength (σ_t) and initial pore pressure (P_0) were selected as the influential factors to be investigated in this paper (see Table 3). The stress ratio (σ_1/σ_2) is between 1.33 and 2.0 in most regions of a coal seam (Yu and Zheng, 1983), so we selected a variation range from 1.0 to 1.9. Based on real examples of coal seams, we selected variation ranges of 6.2 to 14.2 MPa for the minimum horizontal principal stress, 1.7 to 2.3 MPa for the tensile strength, and 4 to 8 MPa for the initial pore pressure. The orthogonal design schemes and the calculated results for the breakdown pressure are given in Table 4.

The injection flow rate and injection time were selected to be 8.676 m^3/h and 400 s, respectively. It can be seen from the injection-pressure curve (see Fig. 11) that with continuous injection, the injection pressure gradually increases from the initial pore pressure to a peak value and then suddenly decreases. This is mainly due to the initial cracks that have already formed at that time and some of the liquid near the injecting hole filling the cracks, which leads to a sudden drop in the injection pressure. The peak value is referred to as the breakdown pressure. With successive injection from the outside, the liquid collects in the injecting hole and the previous formed cracks. New cracks will be generated in the coal seam over time, causing the injection pressure to drop again. Consequently, the injection-pressure curve is therefore a serrated profile with the continued crack propagation.

The results of HF numerical calculation show that the breakdown pressure is influenced by the combined effects of the maximum and minimum horizontal principal stresses, the tensile strength and the initial pore pressure. The empirical formula for the breakdown pressure as a function of these four factors, which is shown in Eq. (10), was obtained via regression analysis. The HF simulation results for the regression analysis are given in Table 4. It can be seen that the breakdown pressure exhibits a positive linear correlation with the minimum horizontal principal stress and the tensile strength and exhibits a negative linear correlation with the maximum horizontal principal stress and the initial pore pressure. The initial stress conditions play an important role in HF, the greater the minimum horizontal principal stress is, the larger the breakdown pressure will be. As the ratio between the maximum and minimum horizontal principal stresses decreases, the breakdown pressure will in contrast increase. Du (2008) also have found that assuming a certain burial depth of coal seam, with the increase of stress ratio (σ_1/σ_2), namely the increase of the horizontal principal stress difference, breakdown pressure would gradually reduce when simulating the hydraulic fracturing of coal bed. Therefore, a higher probability of a successful

Table 3
Influential factors that can change the breakdown pressure.

Stress ratio σ_1/σ_2	Minimum horizontal principal stress σ_2 (MPa)	Tensile strength σ_t (MPa)	Initial pore pressure P_0 (MPa)
1.0	6.2	1.7	4
1.3	7.2	1.8	5
1.5	9.2	2.0	6
1.7	11.2	2.2	7
1.9	14.2	2.3	8

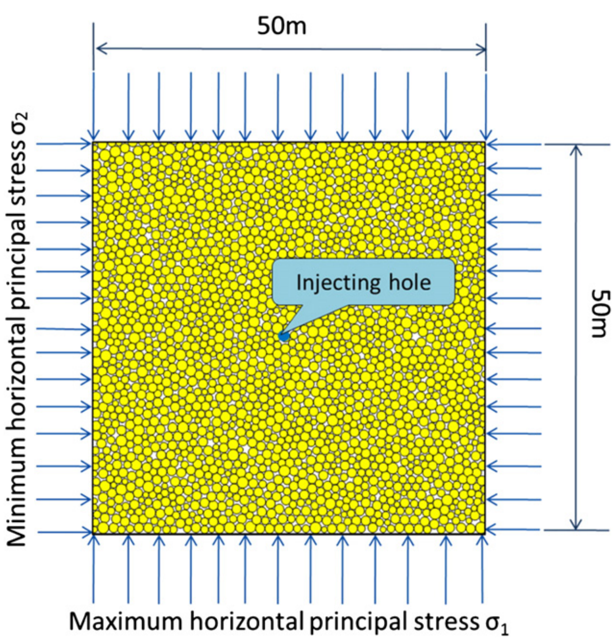

Fig. 10. PFC^{2D} model prior to injection.

Table 4
Orthogonal simulations and results of the breakdown-pressure with varying parameters.

Number	Stress ratio σ_1/σ_2	Minimum horizontal principal stress σ_2 (MPa)	Tensile strength σ_t (MPa)	Initial pore pressure P_0 (MPa)	Breakdown pressure P_b (MPa)
1	1.3	7.2	2.3	4	48.36
2	1.9	14.2	1.8	4	68.34
3	1.5	11.2	2.3	5	58.33
4	1.9	7.2	2.2	6	39.95
5	1.0	14.2	2.3	8	64.51
6	1.9	9.2	2.3	7	43.61
7	1.3	6.2	2.2	8	30.81
8	1.5	7.2	2.0	8	30.93
9	1.5	6.2	1.8	7	28.22
10	1.0	6.2	1.7	4	39.01
11	1.7	6.2	2.3	6	36.39
12	1.7	7.2	1.7	7	30.62
13	1.3	14.2	2.0	7	69.67
14	1.0	11.2	2.2	7	56.78
15	1.9	6.2	2	5	38.90
16	1.5	9.2	2.2	4	53.13
17	1.7	11.2	2.0	4	64.65
18	1.0	9.2	2.0	6	48.14
19	1.5	14.2	1.7	6	67.61
20	1.0	7.2	1.8	5	41.44
21	1.3	11.2	1.8	6	57.33
22	1.7	9.2	1.8	8	36.92
23	1.3	9.2	1.7	5	50.76
24	1.9	11.2	1.7	8	42.93
25	1.7	14.2	2.2	5	68.57

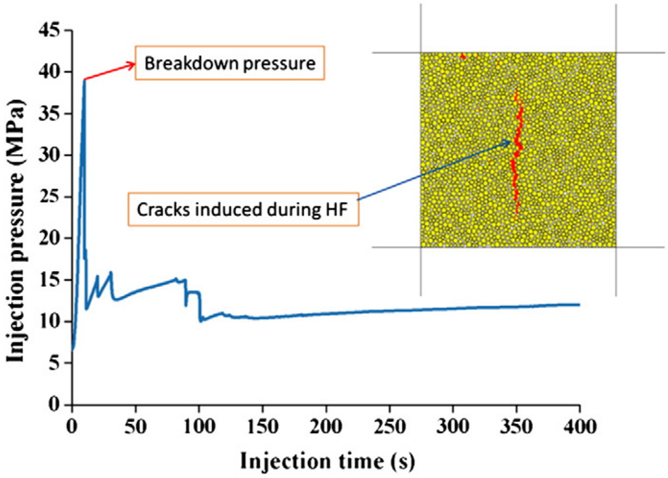

Fig. 11. Injection-pressure history and cracks induced during HF.

fracturing condition exists in a higher initial stress ratio of the coal seam. The existence of an initial pore pressure is conducive to the fracturing of the coal seam, the larger the initial pore pressure, the smaller the breakdown pressure. Considering the main type of cracking in coal-seam HF to be tensile, the fracturing of the coal seam must overcome the tensile strength. Therefore, the breakdown pressure will increase with an increase in tensile strength.

$$P_b = a\sigma_t - \sigma_1 + c\sigma_2 - P_0 \tag{10}$$

where a is equal to 6.985, c is equal to 5.713, and the correlation coefficient is equal to 0.945.

From the classical Kirsch equations for stress concentration around a circular elastic hole, Hubbert and Willis (1957), Haimson and Fairhurst (1967), Fairhurst (2003), and Haimson and Cornet (2003) have proposed the following equation:

$$P_b = \sigma_t - \sigma_1 + 3\sigma_2 - P_0 \tag{11}$$

It can be seen that while Eqs. (10) and (11) are consistent in form, their coefficients differ. Because Eq. (11) is derived based on the theory of elasticity (it is assumed that rock in an oil-bearing formation is elastic, porous, isotropic and homogeneous (Haimson and Fairhurst, 1967)), it requires a certain degree of correction when it is applied to problems of rock mass.

Some of the breakdown pressures (see Table 4) seem high compared to published data. Zoback et al. (1977) have obtained a breakdown pressure of nearly 60 MPa in laboratory experiments when studying the effect of the pressurization rate. Shimizu et al. (2011) have obtained a breakdown pressure of 40.42 MPa when using DEM to simulate HF. Based on many numerical simulation models, our explanation for the discrepancy among the results is that our model is larger in size than theirs, and the size of the model will influence the value of the breakdown pressure, which is our next subject of research.

4.2. Major influential factors with respect to the fracture radius

The mechanical properties of a coal seam determine the crack propagation process during HF under the condition that external factors such as the injection flow rate and injection time remain stable. The influence of macro-mechanical parameters on the crack propagation is discussed in this section. The macro-elastic modulus (from 0.1 to 6.0 GPa), Poisson's ratio (from 0.15 to 0.4), the UCS (from 7.8 to 12.3 MPa), and the tensile strength (from 1.7 to 2.6 MPa) were selected as variables to define various test schemes. The main macro-mechanical parameters that influence the fracture radius were analyzed according to numerical simulations of HF.

It can be seen from the crack distribution (see Fig. 11) that the cracks expand from the injection hole toward both ends of the model during the fracturing process. At the end of fracturing, two fracture-radius values can be obtained by calculating the distance from the injection hole to each end of the crack; the final fracture radius is the average of the two values.

As shown in Fig. 12, the fracture radius generally increases as the macro-elastic modulus increases. The curve of the fracture radius vs. Poisson's ratio (see Fig. 13) shows that the fracture radius also increases as Poisson's ratio increases.

The matching function can be obtained by using the simulation results for regression analysis (see Eq. (12)). The correlation coefficients were found to be 0.995 and 0.998 for the relations of the fracture radius to the macro-elastic modulus and Poisson's ratio, respectively. The fracture radius has a power-function relation with the macro-elastic modulus when Poisson's ratio is constant, and the fracture radius has a linear relationship with $\frac{1}{\sqrt{1-\nu^2}}$ when the macro-elastic modulus is constant.

$$L = \begin{cases} k\sqrt{E} \\ \dfrac{\lambda}{\sqrt{1-\nu^2}} - \lambda_0 \end{cases} \tag{12}$$

where L is the fracture radius (in m), E is the macro-elastic modulus (in Pa), k is equal to 0.000303, λ is equal to 145.005, and λ_0 is equal to135.806.

Wu and Tu (1995) have derived the crack size of an elliptical cross section with constant height according to the displacement field equation of type mode I cracks under a plane-strain condition based on linear elastic fracture mechanics:

$$L = \sqrt{\frac{Eqt}{2Hp\pi(1-\nu^2)}} \tag{13}$$

where E is the macro-elastic modulus (in Pa), q is the injection flow rate (in m^3/s), t is the injection time (in s), H is the thickness of the coal seam (in m), p is the fluid pressure inside the crack (in Pa), and ν is Poisson's ratio.

It can be seen that Eq. (12) is consistent with Eq. (13) in form, and the fracture radius is linearly proportional to $\sqrt{E}$ and $\frac{1}{\sqrt{1-\nu^2}}$.

The simulation results of the HF model demonstrate that changes in the tensile strength have little effect on the fracture radius, which remains at approximately 18 m and can be viewed as a constant. It can be concluded that the fracture radius has little correlation with the

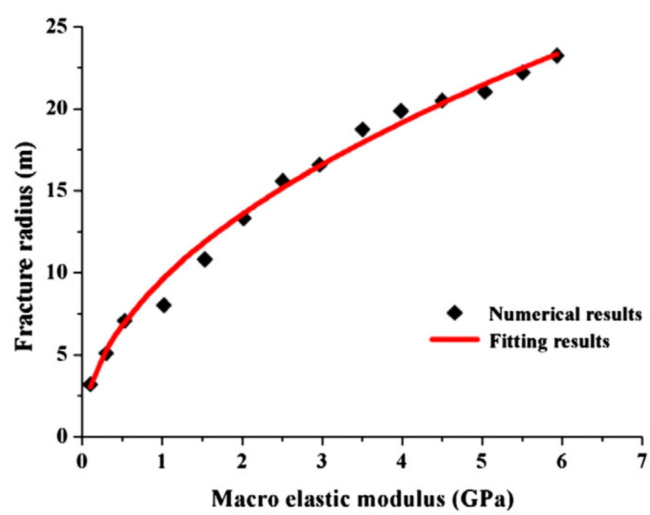

Fig. 12. Simulated relationship between the fracture radius and macro-elastic modulus.

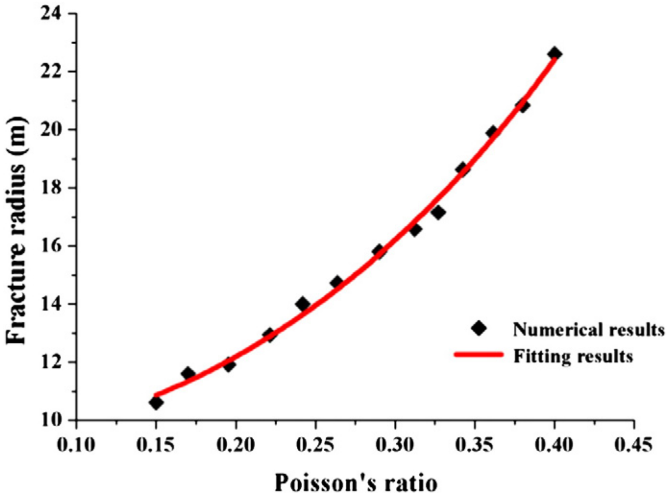

Fig. 13. Simulated relationship between the fracture radius and the Poisson's ratio.

tensile strength. Meanwhile, with an increase in the UCS, the fracture radius exhibits no clear trend of increase or decrease but fluctuates between approximately 19 m and 21 m. It is concluded that the relationship between the UCS and the fracture radius is also weak. Therefore, we suggest that the macro-elastic modulus and Poisson's ratio are the main factors influencing the fracture radius. The rule of simulation results agrees with the traditional KGD and PKN fracture models (Daneshy, 1973; Geertsma and de Klerk, 1969; Perkins and Kern, 1961; Wu and Tu, 1995).

5. Study of injection parameters that affect crack propagation

The performance of HF is primarily influenced by the injection flow rate, the injection time and the injection pressure. The injection flow rate is an important factor that can directly determine the success and economic efficiency of HF. If the flow rate selected is too large, the creation of new cracks is the main effect, and the length extension and aperture broadening of the cracks are rather weak. Therefore, the speed of crack formation is too high and does not allow the original cracks to be sufficiently extended and broadened. As a result, the newly formed and original cracks cannot generate a connective network for gas transport, and therefore the fracturing has little effect on gas extraction. However, if the flow rate is too small, it is necessary to increase the injection time to achieve the predetermined total volume of injected fluid, which leads to extending the schedule for the HF simulation. The injection time is vital in controlling the engineering quantities and progress. If it is too short, the injection pressure and injection flow must be increased to obtain the desired result, which places higher demand on the HF equipment. Thus, the corresponding cost of the HF process increases. However, although a longer injection time allows the corresponding injection pressure and flow rate to be reduced, an excessively long engineering period is disadvantageous for controlling the engineering quantities and the construction progress.

The injection pressure is also an important factor that influences the effect of HF. In practical engineering projects, the initial injection pressure is often set first, and then the pressure is increased gradually from this value. When the injection pressure surpasses the breakdown pressure, the coal seam will be fractured. The fluid-injection pump will stop injecting fluid when the intended effect of HF is reached. Thus, the injection pressure does not remain constant throughout the entire HF process and is changed with time. Because the injection pressure is directly related to the injection flow rate and the injection time, we mainly study the influence of the injection flow rate and the injection time on the HF process.

In this work, the injection flow rate (from 5.076 to 17.676 m^3/h) and the injection time (from 400 to 700 s) were chosen as variables to study the effect of the injection parameters on crack propagation. A series of parameter combinations was chosen to conduct numerical simulations of HF. The fracture radii were recorded to show the influence of the injection parameters. Based on the simulation results, the curves shown in Figs. 14 and 15 represent the variation in fracture radius with respect to injection time and injection flow rate, respectively.

Clearly, the regular linear relationships depicted in Figs. 14 and 15 are similar. When the injection flow rate is held constant, there exists a linear relation between the fracture radius and the injection time. Meanwhile, the radius linearly increases with the injection flow rate when the injection time remains unchanged. Therefore, the fracture radius has a clear positive correlation with both the injection time and the injection flow rate. The conclusion from the simulation is consistent with the previous research results (Geertsma and de Klerk, 1969; Perkins and Kern, 1961).

Based on the relationships presented above, an expression representing the linear relationship between the fracture radius and the injection parameters (injection flow rate and injection time) can be obtained, as shown in Eq. (14). The correlation coefficient was found to be 0.95.

$$L = aq + bt \tag{14}$$

where L is the fracture radius (in m), q is the injection flow rate (in m^3/h), t is the injection time (in s), $a = 0.98$, and $b = 0.013$. It should be noted that the parameters of the formula are only applicable to this specific model, but the form has a certain degree of universality.

6. Engineering application

Yuyang Coal Mine (YCM), which was built in 1966 and commenced production in 1971, uses an inclined-shaft mining method, with a designed annual output of 450 thousand tons. The mine surface plant, the main and secondary inclined shafts and the main return airway are located at Jinji Yan. The secondary mine surface plant is located in Yangjia Gulf, where a pair of secondary inclined shafts and a main return-air inclined shaft were built. The main haulage roadway, which is 40 m below the M_{12} coal seam, was placed in the limestone strata of the Maokou formation. The thin and moderately thick seams are primarily excavated using fully mechanized mining techniques, which include mechanical ventilation, water-pump drainage, a conveyor belt for continuous coal transportation, an electric locomotive for gangue transportation, winch hoisting, and miner's lamp lighting.

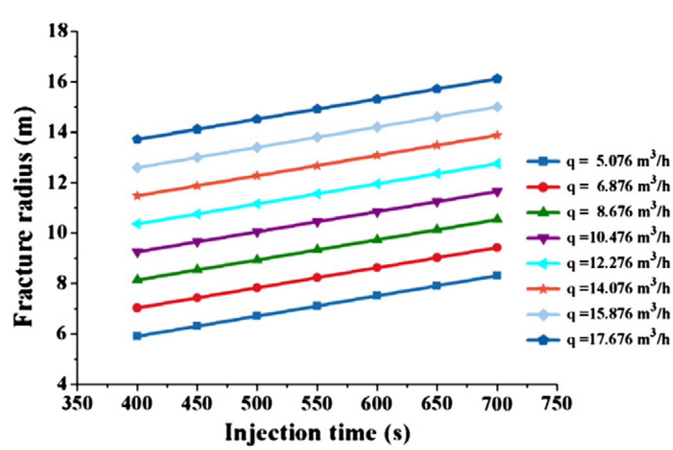

Fig. 14. Relationship between the fracture radius and the injection time for various injection flow rates.

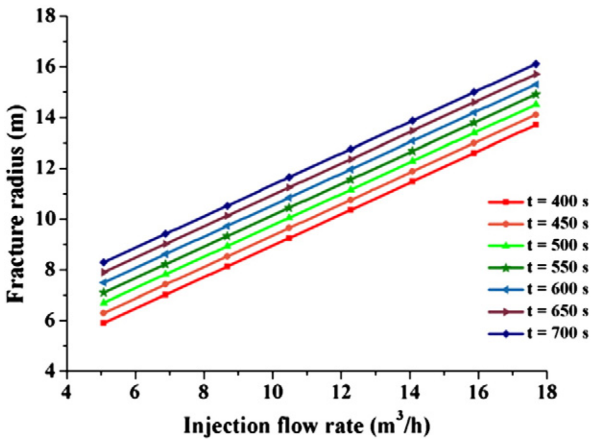

Fig. 15. Relationship between the fracture radius and the injection flow rate for various injection times.

6.1. Stratigraphic information and fracturing technology

The fracturing coal seam is in the Permian Longtan formation. A generalized stratigraphic column showing the coal seam and the roof and floor strata is presented in Fig. 16. The coal strata consist of sandstone, argillaceous rock and coal. Sandstone is semi-hard to hard rock and has good integrity. Its strength is affected by the cementation quality and the degree of fracture. Sandy mudstone is semi-hard to weak rock; its integrity is also good. Mudstone and coal are weak rocks. Mudstone is easily weathered; it has weak resistance to softening, collapse and fragmentation under the influence of water, and its integrity is poor. Cracking along the bedding and inflation will appear once sandy mudstone and mudstone have been saturated. Their water stability is poor. The average thickness of the coal seam M_7, which is the target fracturing layer, is 0.86 m, and the bedding and cleat are well developed.

A cross-layer borehole is used for the HF process. The fracturing fluid is a water-based fracturing fluid. The fracturing equipment includes pumping units (Halliburton), blenders, bulk handling equipment and a manifold trailer. The HF of M_7 at YCM was begun on April 19th, 2001, and the fracturing time was 10.5 h.

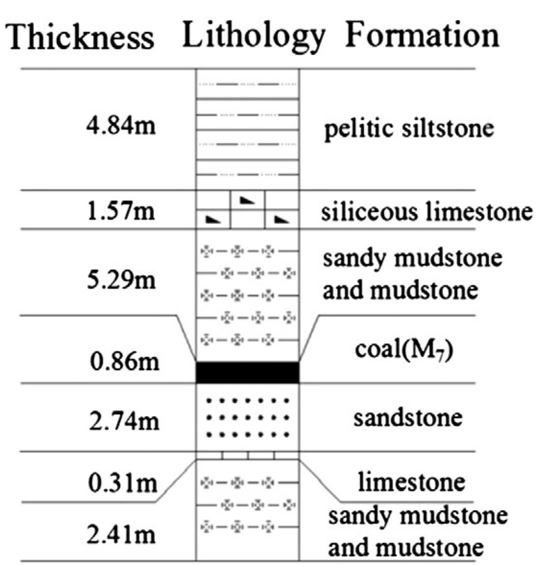

Fig. 16. A generalized stratigraphic column representing the coal mine.

6.2. Selection of mechanical parameters and fracturing parameters

The mechanical parameters were adopted from the engineering geological exploration data from working face N3704 at YCM. The values shown in Table 5 are the selected mechanical parameters, which were obtained from a combination of engineering experience and related literature and considered alongside the repeated comparison, analysis, simulation tests, calibration, and characteristics of the PFC^{2D} numerical method. The numerical calculation model is shown in Fig. 17. The model was 150 m in length and 75 m in width. The particle radius was chosen to have a uniform distribution between the maximum and minimum radii. The minimum radius was 0.42 m, the ratio of the largest to the smallest radius was 1.66, and the porosity was 0.15. The number of particles in the model was 10,588. It should be noted that discontinuities of the coal are not discussed in this paper; this topic should be the focus of subsequent research.

In the preceding discussions, it was established that during numerical simulations using PFC^{2D}, the meso-mechanical parameters must be specified, and they can be derived from macro-mechanical parameters. The numerical model reflecting the macro-parameters can then be established. Using the previously established quantitative relationships between the macro-mechanical parameters and the meso-mechanical parameters, the PFC^{2D} input parameters that correspond to the macro-mechanical parameters of the coal seam can be obtained as shown in Table 5.

Studies have shown that the injection parameters (injection pressure, injection time, injection flow rate, etc.) are not only directly related to the performance of HF but also have a significant influence on the benefit of fracturing construction (economic benefit, schedule control, etc.). According to the raw HF data from the working face N3704 at YCM and considering that the fracturing-fluid efficiency is approximately 12%, the fracturing parameters are finally selected on the basis of model test studies (see Table 6).

6.3. Comparison between the results of the numerical simulation and the field observations

By performing numerical simulations of the fracturing process of working face N3704 at YCM, we obtained a series of numerical simulation results. This section compares the results of the numerical simulation to the actual effects recorded in the HF field observations, and the applicability of the numerical algorithm for HF is verified.

Table 5
Values of the macro-mechanical parameters of the coal seam and the meso-mechanical parameters used in the PFC^{2D} simulation.

Macro-mechanical parameters	
Tensile strength (MPa)	2.0
Uniaxial compressive strength (MPa)	10.3
Elastic modulus (GPa)	2.97
Poisson's ratio	0.32
Internal friction angle	35.4°
Density (kg/m^3)	1390
PFC^{2D} model input parameters	
Minimum particle radius (m)	0.42
Particle radius ratio	1.66
Particle density (kg/m^3)	1635
Particle friction coefficient	0.71
Particle contact Young's modulus (GPa)	2.4
Parallel bond Young's modulus (GPa)	2.4
Parallel bond shear strength (MPa)	7.0
Parallel bond normal strength (MPa)	7.0
Ball-contact normal-to-shear stiffness ratio	2.5
Parallel-bond normal-to-shear stiffness ratio	2.5

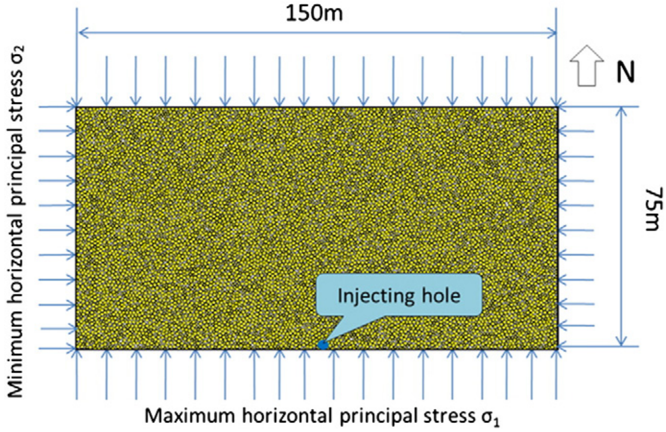

Fig. 17. Numerical PFC^{2D} model.

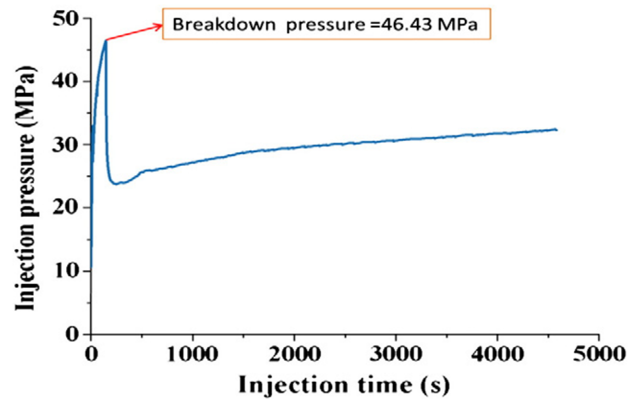

Fig. 18. Simulated relationship between the injection pressure and the injection time.

According to the field HF data for the working face N3704 at YCM, the actual breakdown pressure is 45.10 MPa, and the result of the numerical simulation is 46.43 MPa (see Fig. 18). It can be seen that the result of the numerical simulation is in agreement with the field measurement, and the numerical simulation based on particle flow reflects the characteristics of crack initiation under the action of HF.

Based on the hydraulic fracturing data from the working face N3704, it can be found that the observed fracture radii measured from the injecting hole in the northern and southern directions are between 60 and 70 m. The result from the numerical simulation shows a fracture radius of 65.10 m in the northern direction (see Fig. 19), and considering the symmetry of the fracturing effect, the fracture radius in the southern direction should be close to this value. Thus it can be seen that the result of the simulation agrees with the actual condition. This comparison indicates that the HF numerical simulation based on the PFC^{2D} method can realistically model the crack propagation features observed for the coal seam in-situ.

6.4. Verification of the empirical formulae

Earlier in the paper we proposed empirical formulae for the breakdown pressure as a function of the initial stress, initial pore pressure and tensile strength and for the fractured radius as a function of the injection flow rate and injection time. The reliability of these formulae for the working face N3704 is verified in this section.

The breakdown pressure can be calculated by substituting the corresponding parameters ($\sigma_t = 2$ MPa, $\sigma_1 = 13.88$ MPa, $\sigma_2 = 9.25$ MPa, and $P_0 = 6.64$ MPa) into the established empirical formula for the breakdown pressure (Eq. (10)). The value calculated in this way is 46.3 MPa, which is close to the value (45.1 MPa) measured in the field. This agreement illustrates that the empirical formula is applicable for predicting the breakdown pressure of a coal seam.

Based on the information from the field tests of HF, by substituting the selected injection parameters ($q = 10.48$ m^3/h, $t = 4580$ s) into the calculated fracture radius regression model Eq. (14), the fracture radius can be calculated ($L = 69.81$ m). This result is close to the field result. It is clear that the results calculated using the proposed empirical formulae are consistent with those measured in the actual mine formation of HF.

Table 6
Fracturing parameters.

Total injection time (s)	37,800
Effective injection time (s)	4580
Injection flow rate (m^3/h)	10.48
The initial injection pressure (MPa)	6.64

7. Conclusions

(1) Based on numerous numerical simulations, this paper studies the link between macro-mechanical parameters and meso-mechanical parameters and then establishes empirical equations that describe the relationships. It is found that the macro-elastic modulus of a material has positive linear and negative logarithmic relationships with the meso-Young's modulus and normal-to-shear stiffness ratio of its constituent particles, respectively. The Poisson's ratio presents logarithm relevant to the normal-to-shear stiffness ratio of the particles. The UCS and tensile strength are related to the parallel-bond strength. In summary, the mesoscopic modulus is mainly related to the macroscopic modulus, and the mesoscopic strength is mainly related to the macroscopic strength.

(2) According to the empirical equations that describe the relationship between macro-mechanical parameters and meso-mechanical parameters, the meso-mechanical parameters can be determined from the macro-mechanical parameters measured in laboratory tests. Preliminary meso-mechanical parameters are then chosen for the numerical tests, and calibrated through comparison with the measured macro-mechanical parameters. It is found that the difference between the calculated meso-mechanical parameters and the meso-mechanical parameters obtained from calibration is small, which confirms the reliability of the empirical equations.

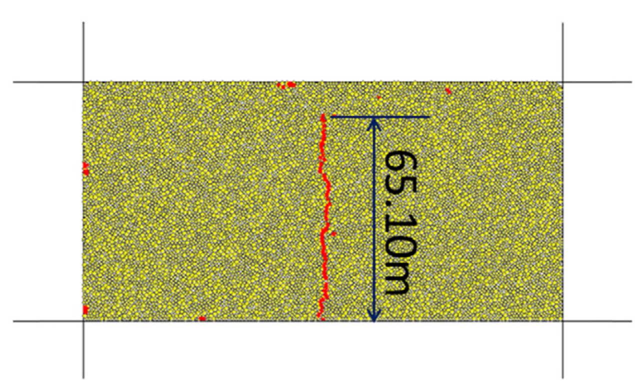

Fig. 19. Crack distribution of the HF simulation.

(3) Multiple parameter combinations were designed to study the influence of macro-mechanical parameters and initial stress on HF. The breakdown pressure and the fracture radius were chosen as the criteria for assessing the performance of the HF process. It is found that the initial stress conditions and the tensile strength have a direct influence on the value of the breakdown pressure, which has a positive linear relationship with the minimum horizontal principal stress and the tensile strength and has a negative linear relationship with the maximum horizontal principal stress and the initial pore pressure. The fracture radius is primarily influenced by the macro-elastic modulus and Poisson's ratio, and it has a positive nonlinear correlation with both.
(4) The injection flow rate and the injection time exert significant influences on HF. According to the simulation results, the fracture radius is controlled by both the injection flow rate and the injection time, with a positive relationship. On the basis of this finding, empirical formula is provided to describe the relationship between the fracture radius and the injection parameters.
(5) The HF process for the working face N3704 at YCM was simulated. The research results indicate that the breakdown pressure and fracture radius obtained from the numerical simulation agree closely with those measured in the field. It is concluded that PFC^{2D} can be effectively applied to investigate and simulate the process of crack initiation and propagation. Meanwhile, the empirical formulae are reliable for predicting the fracturing effects in practical HF process.

Acknowledgments

The authors would like to thank the Editor and two anonymous reviewers for their helpful and constructive comments. This study was funded by the China Scholarship Council (CSC), by the Major Program of the Major Research Plan of the National Natural Science Foundation of China (NSFC) under Contract No. 91215301-5, and by the NSFC under Contract No. 51304237.

References

Abass, H.H., Hedayati, S., Meadows, D.L., 1990. Experimental observations of hydraulic fracture propagation through coal blocks. Paper SPE 21289 Presented at the SPE Eastern Regional Meeting, Columbus, OH, pp. 239–252.
Abass, H.H., Hedayati, S., Meadows, D.L., 1992. Nonplanar fracture propagation from horizontal wellbore: experimental study. Paper SPE 24834 Presented at the 67th ANNUAL SP Meeting, Washington D.C., pp. 133–137.
Adachi, J., Siebrits, E., Peirce, A., Desroches, J., 2007. Computer simulation of hydraulic fractures. Int. J. Rock Mech. Min. Sci. 44, 739–757.
Aghighi, M.A., Rahman, S.S., 2010. Horizontal permeability anisotropy: effect upon the evaluation and design of primary and secondary hydraulic fracture treatments in tight gas reservoirs. J. Pet. Sci. Eng. 74, 4–13.
Al-Busaidi, A., Hazzard, J.F., Young, R.P., 2005. Distinct element modeling of hydraulically fractured Lac du Bonnet granite. J. Geophys. Res. Solid Earth 110 (B6), 1–14 (B06302).
Cai, M., Chen, C., Peng, H., Ji, H., Qao, L., Tan, Z., 2006. In-situ stress measurement by hydraulic fracturing technique in deep position of Wangfu coal mine. Chin. J. Rock Mech. Eng. 5, 1069–1074.
Cho, N., Martin, C.D., Sego, D.C., 2007. A clumped particle model for rock. Int. J. Rock Mech. Min. Sci. 44, 997–1010.
Cipolla, C.L., Wright, C.A., 2000. Diagnostic techniques to understand hydraulic fracturing: what? why? and how? SPE Paper 59735 Presented at the 2000 SPE/CERI Gas Technology Symposium. Calgary, Alberta Canada, pp. 1–13.
Cundall, P.A., 1971. A computer model for simulating progressive large scale movements in blocky rock systems. Proceedings of the Symposium of the International Society of Rock Mechanics Nancy, France, II-8, pp. 1–10.
Cundall, P.A., Strack, O.D.L., 1979. A discrete numerical model for granular assemblies. Geotechnique 29, 47–65.
Daneshy, A., 1973. On the design of vertical hydraulic fractures. J. Pet. Technol. 25 (1), 83–97 (paper SPE 3654).
Du, C., 2008. Study on Theoretics of Hydraulic Fracturing in Coal Bed and Its Application. (PhD thesis) China University of Mining and Technology.
Du, C., Mao, X., Bu, W., 2008. Analysis of fracture propagation in coal seams during hydraulic fracturing. J. Min. Saf. Eng. 2, 231–234.
Fairhurst, C., 2003. Stress estimation in rock: a brief history and review. Int. J. Rock Mech. Min. Sci. 40 (7–8), 957–973.
Fisher, M.K., Warpinski, N.R., 2012. Hydraulic-Fracture-Height growth: real data. SPE Paper 145949, 27(1), pp. 8–19.
Geertsma, J., de Klerk, F., 1969. A rapid method of predicting width and extent of hydraulically induced fractures. J. Pet. Technol. 21 (12), 1571–1581 (paper SPE 2458).
Haimson, B.C., Cornet, F.H., 2003. ISRM Suggested Methods for rock stress estimation-Part 3: hydraulic fracturing (HF) and/or hydraulic testing of pre-existing fractures (HTPF). Int. J. Rock Mech. Min. Sci. 40 (7–8), 1011–1020.
Haimson, B.C., Fairhurst, C., 1967. Initiation and extension of hydraulic fractures in rock. Soc. Pet. Eng. J. 7, 310–318.
Han, Y., Cundall, P.A., 2011. Lattice Boltzmann modeling of pore-scale fluid flow through idealized porous media. Int. J. Numer. Methods Fluids 67 (11), 1720–1734.
Han, Y., Cundall, P.A., 2013. LBM–DEM modeling of fluid–solid interaction in porous media. Int. J. Numer. Anal. Methods Geomech. 37 (10), 1391–1407.
Han, Y., Damjanac, B., Nagel, N., 2012. A microscopic numerical system for modeling interaction between natural fractures and hydraulic fracturing. Proceedings of the 46th US Rock Mechanics/Geomechanics Symposium, Chicago, IL.
Hoffman, B.T., Chang, W.M., 2009. Modeling hydraulic fractures in finite difference simulators: application to tight gas sands in Montana. J. Pet. Sci. Eng. 69, 107–116.
Hossain, M.M., Rahman, M.K., 2008. Numerical simulation of complex fracture growth during tight reservoir stimulation by hydraulic fracturing. J. Pet. Sci. Eng. 60, 86–104.
Hubbert, K.M., Willis, D.G., 1957. Mechanics of hydraulic fracturing. Pet. Trans. AIME 210, 153–166.
Itasca Consulting Group Inc., 2010. PFC2D-Particle Flow Code in two dimensions. Ver. 4.0 User's Manual.ICG, Minneapolis.
Jeffrey, R.G., Mills, K.W., 2000. Hydraulic fracturing applied to inducing longwall coal mine goaf falls. Proceedings of the 4th American Rock Mechanics Symposium, Seattle, Washington, D.C., pp. 423–430.
Jeffrey, R.G., Weber, C.R., Vlahovic, W., Enever, J.R., 1994. Hydraulic fracturing experiments in the great northern coal seam. Proceedings of the 1994 SPE Asia Pacific Oil & Gas Conference, Melbourne, Australia, pp. 361–371.
Krajcinovic, D., 2000. Damage mechanics: accomplishments, trends and needs. Int. J. Solids Struct. 37 (1–2), 267–277.
Kulatilake, P.H.S.W., Malama, B., Wang, J., 2001. Physical and particle flow modeling of jointed rock block behavior under uniaxial loading. Int. J. Rock Mech. Min. Sci. 38, 641–657.
Lemos, J.V., 1987. A Distinct Element Model for Dynamic Analysis of Jointed Rock with Application to Dam Foundations and Fault Motion. (PhD. thesis) University of Minnesota.
Lemos, J.V., Lorig, L.J., 1990. Hydromechanical modelling of jointed rock masses using the distinct element method. Mechanics of Jointed and Faulted Rock, Balkema, Rotterdam. 605–612.
Li, G., Ye, Q., Li, J., Xu, S., Pan, F., Lian, J., Wu, S., 2010. Theoretical analysis and practical study on reasonable water pressure of hydro-fracturing technology. China Saf. Sci. J. 20 (12), 73–78.
McLennan, J., Tran, D., Zhao, N., Thakur, S., Deo, M., Gil, I., Damjanac, B., 2010. Modeling fluid invasion and hydraulic fracture propagation in naturally fractured rock: a three-dimensional approach. Presented at International Symposium and Exhibition on Formation Damage Control, Lafayette, LA, pp. 1–13.
Papanastasiou, P.C., 1997. A coupled elastoplastic hydraulic fracturing model. Int. J. Rock Mech. Min. Sci. 34, 240–241.
Perkins, T.K., Kern, L.R., 1961. Widths of hydraulic fractures. J. Pet. Technol. 13 (9), 937–949 (paper SPE 89 presented at the 36th Annual Fall Meeting SPE, Dallas, TX).
Potyondy, D.O., Cundall, P.A., 2004. A bonded-particle model for rock. Int. J. Rock Mech. Min. Sci. 41 (8), 1329–1364.
Rahim, Z., Holditch, S.A., Zuber, M.D., Buehring, D., 1995. Evaluation of fracture treatments using a layered reservoir description: field examples. J. Pet. Sci. Eng. 12 (4), 257–267.
Schlangen, E., Garboczi, E.J., 1997. Fracture simulations of concrete using lattice models: computational aspects. Eng. Fract. Mech. 57 (2–3), 319–332.
Shimizu, Y., 2004. Fluid Coupling in PFC2D and PFC3D. Proceedings of the 2nd International PFC Symposium, Kyoto, Japan, Minneapolis, MN, pp. 281–287.
Shimizu, H., 2010. Distinct Element Modeling for Fundamental Rock Fracturing and Application to Hydraulic Fracturing. (PhD thesis) Kyoto University.
Shimizu, H., Murata, S., Ishida, T., 2011. The distinct element analysis for hydraulic fracturing in hard rock considering fluid viscosity and particle size distribution. Int. J. Rock Mech. Min. Sci. 48, 712–727.
Tawadrous, A.S., DeGagné, D., Pierce, M., Mas Ivars, D., 2009. Prediction of uniaxial compression PFC^{3D} model micro-properties using artificial neural networks. Int. J. Numer. Anal. Methods Geomech. 33 (18), 1953–1962.
Tsuji, Y., Tanaka, T., Ishida, T., 1992. Lagrangian numerical simulation of plug flow of cohesionless particles in a horizontal pipe. Powder Technol. 71, 239–250.
Tsuji, Y., Kawaguchi, T., Tanaka, T., 1993. Discrete particle simulation of two-dimensional fluidized bed. Powder Technol. 77 (1), 79–87.
Vychytil, J., Horii, H., 1998. Micromechanics-based continuum model for hydraulic fracturing of jointed rock masses during HDR stimulation. Mech. Mater. 28, 123–135.
Wang, T., 2008. Research on simulation of rupture of rock mass around tunnels based on PFC. The First International FLAC/DEM Symposium on Numerical Modeling, Minneapolis, MN, pp. 565–570.
Wang, Y., Tonon, F., 2009. Modeling Lac du Bonnet granite using a discrete element model. Int. J. Rock Mech. Min. Sci. 46 (7), 1124–1135.
Wang, J.G., Zhang, Y., Liu, J.S., Zhang, B.Y., 2010. Numerical simulation of geofluid focusing and penetration due to hydraulic fracture. J. Geochem. Explor. 106, 211–218.
Warpinski, N.R., 1985. Measurement of width and pressure in a propagating hydraulic fracture. SPE Paper 11648, 25(1), pp. 46–54.
Wright, C.A., Conant, R.A., 1995. Hydraulic fracture reorientation in primary and secondary recovery from low-permeability reservoirs. Paper SPE 30484 Presented at the 1995 ANNUAL Technical Conference and Exhibition, Dallas, TX, pp. 357–369.

Wu, X.M., Tu, H.Z., 1995. Morphological analysis and geometrical size determination of representative hydraulic fractures in coal seam. Earth Sci.-J. China Univ. Geosci. 1, 112–116.
Yoon, J., 2007. Application of experimental design and optimization to PFC model calibration in uniaxial compression simulation. Int. J. Rock Mech. Min. Sci. 44 (6), 871–889.
Yu, X., Zheng, Y., 1983. Stability Analysis of Surrounding Rock of Underground Engineering. Coal industry publishing house (48 pp.).
Zhang, G.M., Liu, H., Zhang, J., Wu, H.A., Wang, X.X., 2010. Three-dimensional finite element simulation and parametric study for horizontal well hydraulic fracture. J. Pet. Sci. Eng. 72, 310–317.
Zoback, M.D., Rummel, F., Jung, R., Raleigh, C.B., 1977. Laboratory hydraulic fracturing experiments in intact and pre-fractured rock. Int. J. Rock Mech. Min. Sci. Geomech. Abstr. 14 (2), 49–58.